Electronic properties of transition metal atoms on Cu₂N/Cu(100)

A. Ferrón,[1,2] J. L. Lado,[1] and J. Fernández-Rossier[1,3]

[1]*International Iberian Nanotechnology Laboratory (INL), Avenida Mestre José Veiga, 4715-330, Braga, Portugal*
[2]*Instituto de Modelado e Innovación Tecnológica (CONICET-UNNE), Avenida Libertad 5400, W3404AAS Corrientes, Argentina*
[3]*Departamento de Física Aplicada, Universidad de Alicante, San Vicente del Raspeig, 03690 Spain*

We study the nature of spin excitations of individual transition metal atoms (Ti, V, Cr, Mn, Fe, Co, and Ni) deposited on a Cu₂N/Cu(100) surface using both spin-polarized density functional theory (DFT) and exact diagonalization of an Anderson model derived from DFT. We use DFT to compare the structural, electronic, and magnetic properties of different transition metal adatoms on the surface. We find that the average occupation of the transition metal d shell, main contributor to the magnetic moment, is not quantized, in contrast with the quantized spin in the model Hamiltonians that successfully describe spin excitations in this system. In order to reconcile these two pictures, we build a zero bandwidth multi-orbital Anderson Hamiltonian for the d shell of the transition metal hybridized with the p orbitals of the adjacent nitrogen atoms, by means of maximally localized Wannier function representation of the DFT Hamiltonian. The exact solutions of this model have quantized total spin, without quantized charge at the d shell. We propose that the quantized spin of the models actually belongs to many-body states with two different charge configurations in the d shell, hybridized with the p orbital of the adjacent nitrogen atoms. This scenario implies that the measured spin excitations are not fully localized at the transition metal.

I. INTRODUCTION

The Cu(100) surface coated with a Cu₂N monolayer has turned out to be a remarkable system [1–17] to probe and engineer the electronic properties of individual transition metal atoms using scanning tunneling microscopy (STM) and inelastic electron tunneling spectroscopy (IETS). A variety of breakthroughs have been reported on this system, such as the first measurement of the magnetic anisotropy of an individual quantized spin by means of IETS [2], the demonstration of single atom spin torque [5], the fabrication of nano-engineered chains both with antiferromagnetic [7] and ferromagnetic [11] broken symmetry ground states, probed by means of spin-polarized STM, the measurement of spin excitations in spin chains with strong quantum fluctuations that prevent spin symmetry breaking [1,8], the measurement of single spin relaxation time by means of the voltage pulse pump-probe technique [6], the observation of renormalization of magnetic anisotropy due to Kondo exchange interactions [9], and the imaging of spin wave modes with atomic scale resolution [11].

The system has been studied from the theoretical standpoint, using a variety of approaches [2,18–41]. Importantly, both the spin excitation spectra of individual atoms [2,3,14] and multi-atom structures [1,4,7–9,11–13], as well as their spin relaxation dynamics have been successfully described using model Hamiltonians [18–26] where *quantized* spins interact with each other via Heisenberg coupling [1,11,18,20], and are Kondo coupled both to the tunneling electrons [18,19] and to the substrate [9,22–24]. Treating Kondo coupling up to second order in perturbation theory accounts for spin relaxation [22,23] and magnetic anisotropy renormalization [9,24]. Furthermore, calculations [25,26] up to third order are also able to account for nontrivial IETS line shapes, including Kondo peaks. Numerical renormalization group nonperturbative calculations for the anisotropic spin Kondo model also provide very good description for both the finite

energy spin excitations and the zero bias Kondo peak in these systems [21,42,43]. The origin of the Kondo couplings in these systems can be traced down to a multi-orbital Anderson model for these $S > 1/2$ systems [27], in line with the very well known results for the mapping [44–46] of the single orbital Anderson model [47] to the Kondo model.

In spite of the success of quantized spin Hamiltonians to describe many experiments of transition metals on Cu₂N, there is a problem of principle that we address in this paper. Density functional theory (DFT) calculations, most of them [2,21,28–35] dealing with Ti, Mn, Fe, and Co adatoms on Cu₂N/Cu(100), show that nor the charge, neither the magnetic moment of these magnetic atoms are quantized.

Here we provide a comprehensive and comparative study of the electronic and structural properties of the entire series of $3d$ transition metals (Ti, V, Cr, Mn, Fe, Co, and Ni). To the best of our knowledge, no DFT calculations have been reported for V and Ni on Cu₂N/Cu(100). Our calculations confirm the fractional nature of the average occupation of the d levels in these systems, which is not surprising given their conducting nature, but it poses an apparent contradiction with the quantized spin model description. In the second part of the manuscript we provide a solution to this apparent conflict. We build a zero bandwidth multi-orbital Anderson model, using as starting point the representation of the DFT Kohn-Sham Hamiltonian in a basis of maximally localized Wannier functions. The Anderson model includes spin-orbit interactions, crystal field interactions, on-site Coulomb repulsion, and hybridization of the d shell of the transition metal with its nitrogen neighbors. We solve the model by exact numerical diagonalization within a restricted Hilbert space that includes both d^n configurations with $d^{n+1}p^m$ configurations, where n stands for the number of electrons in the d shell and m stands for the number of electrons in the nitrogen p orbitals. Our numerics show that the low energy excitations of the model can be mapped into

quantized spin Hamiltonians. Within this picture, it is apparent that this quantized spin S describes the quantum number of many-body wave functions that mix states with n and $n + 1$ electrons in the d shell, and have thereby noninteger average occupation.

The paper is organized as follows. In Sec. II we describe DFT calculations for different transition metal (TM) atoms at Cu_2N paying particular attention to the structural properties (II B), electronic properties (II C) and magnetic properties (II D). In Sec. III we build the zero bandwidth multi-orbital Anderson model, using as starting point the DFT calculations, and we analyze the connection with the spin models. Finally, Sec. IV contains a summary and a discussion of our most important findings.

II. DENSITY FUNCTIONAL CALCULATIONS

A. Methods

Most of our DFT calculations of $3d$ transition metal adatoms adsorbed on $Cu_2N/Cu(100)$ were done using the generalized-gradient approximation (GGA) and $CGA + U$ for exchange-correlation energy [48], using plane-wave basis sets and the projector augmented-wave (PAW) method [49] as implemented in QUANTUM ESPRESSO (QE) code [50]. Additionally, in some particular cases we have performed complementary calculations using the local spin density approximation (LSDA) [51] for exchange-correlation energy, using the all-electron full-potential linearized augmented-plane wave (FP-LAPW) method as implemented in ELK [52].

In order to test the size convergence, we have used two supercells with different sizes. Both cells have four slabs of $Cu(100)$, separated by a vacuum region of 15 Å. The smaller cell has 37 atoms (1 TM, 4 N, and 32 Cu) and a bigger supercell has 82 atoms (1 TM, 9 N, and 72 Cu). The corresponding structures are shown in Fig. 1. In the smallest structure, the intercell distance between TM atoms along the N direction is 7.2 Å, while in the bigger one this distance is 10.8 Å.
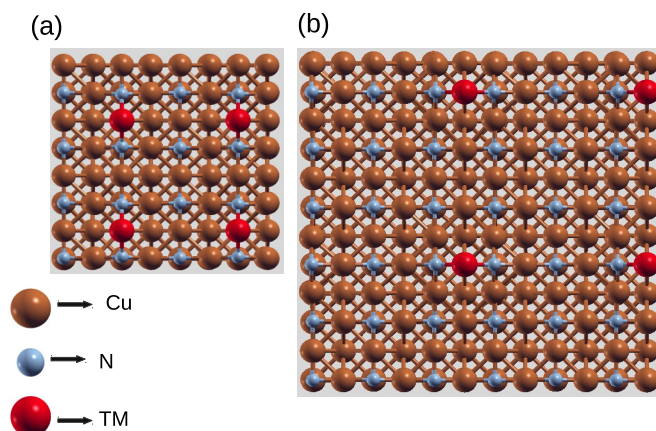

FIG. 1. (Color online) Top view for the structure of the TM@Cu_2N. (a) Small supercell where a, the intercell distance between TM atoms along the N direction, is 7.2 Å. (b) Big supercell, with $a = 10.8$ Å.

QE calculations are done in two stages: structural relaxation and electronic structure calculation. In the relaxation stage, the meshes in k space for the small and big cells were $6 \times 6 \times 1$ and $4 \times 4 \times 1$ respectively. In both cases the relaxation was performed until the forces acting on atoms were smaller than 10^{-3} a.u. In the second stage, the meshes used were $8 \times 8 \times 1$ for the small supercell and $6 \times 6 \times 1$ for the big one. In all the calculations we used a smearing with a broadening parameter of 0.005–0.02 Ry, in line with previous work [21,29,31], and we fixed the cutoff energies for the wave function and charge density at 40–80 Ry and 400–800 Ry respectively. For the ELK calculations, we started from the relaxed structures obtained with QE. In this case the mesh in k space was $4 \times 4 \times 1$, the product of the muffin-tin radius and the momentum cutoff was $R_{MT} k_{\max} = 6$, and we employed the local spin density approximation (LSDA) [51] for exchange correlation and $DFT + U$ with Yukawa screening [53].

In the case of Fe and Co we have also obtained the so-called maximally localized Wannier functions (MLWFs) [54–59] associated with the Bloch states of the DFT calculation, using the package WANNIER90. The Wannier functions form an orthogonal and complete basis set that we can use to describe our system. Importantly, the representation of the Kohn-Sham Hamiltonian in the DFT basis provides an effective tight-binding model to describe the electronic states of the system, that we use as a starting point to build a zero bandwidth multi-orbital Anderson model, as described in Sec. III.

B. Structural properties

We now discuss the structural properties of a single $3d$ TM atom bonded to the Cu site of the $Cu_2N/Cu(100)$ surface. This is the binding site most frequently reported in the literature [2,8,10,29,31–33]. In order to refer to the different TM atoms we shall use indistinctly their chemical formula (Ti, V, Cr, Mn, Fe, Co, Ni) or the nominal charge on the d shell $q_d = 2,3,4,5,6,7,8$.

Cu_2N is known [2,33] to form a weakly buckled square lattice on top of the $Cu(100)$, consistent with our DFT calculations. In all cases considered, the adsorption of the TM introduces a local distortion on the Cu_2N lattice, shown in Fig. 2: the underneath Cu atom is pushed towards the bulk, and the N atoms are pulled out. These results are in line with previous works [21,33,60]. In order to characterize this structural distortion, we introduce three distances: the TM-N distance (d_N), the TM-Cu distance (d_{Cu}), and the TM-surface vertical displacement, z, that we take as the z component of the vector that joins the TM with the farthest Cu surface atom, marked with an arrow in Fig. 2. In addition we also introduce the angle formed by the N-TM-N trimer (θ).

Our calculations, performed both for the small and large supercells (see Fig. 1) show how these structural values are similar for different TM atoms, but with clear and systematic variations as a function of the number of d electrons (as shown in Fig. 3). Whereas both the TM-N and the TM-Cu distances undergo minor variations across the TM series, the θ angle has a much more marked change, going from structures where the TM is clearly a protrusion and the N atoms are weakly detached from surface, for small q_d, to structures where TM
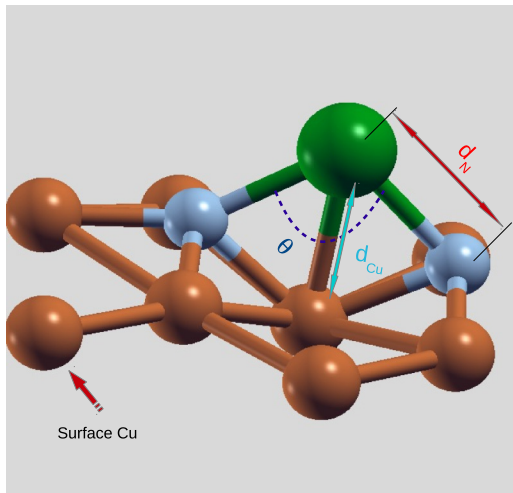
FIG. 2. (Color online) Schematic diagram of the Cu_2N (Cu atoms in brown, N atoms in blue) surface with the TM atom (green). d_N is the distance from the TM atom to the nearest-neighbor N atoms, d_{Cu} refers to the distance from the TM atom to the Cu atom lying just below the magnetic atom, θ is the angle formed by the N-TM-N trimer, and the red arrow shows the position of the Cu atom used to define the surface.

is almost collinear with the N atoms, for Co and Ni. The tendency to form collinear N-TM-N structures is particularly clear in the case of Co and Ni chains (small cells). In the case of Co, the marked difference between the small and big cells suggests that there is a cooperative distortion in the case of cobalt chains along the N direction [17], also visible for Ni, and clearly absent in the case of the lighter TM, such as
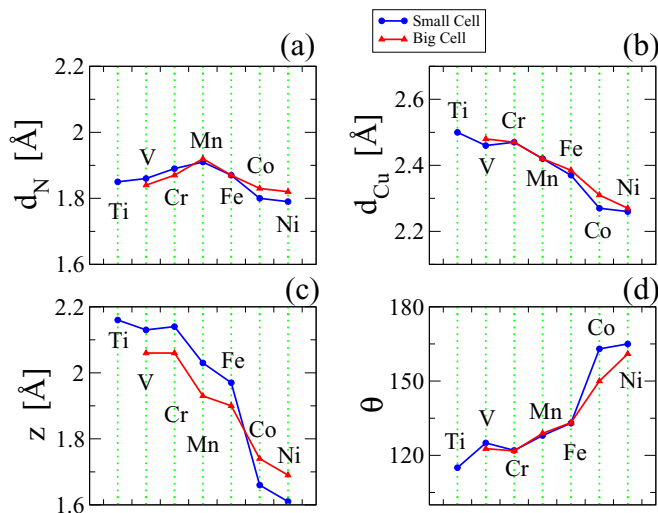
Fe, for which these chains have been studied experimentally [7,8].

C. Electronic properties

We now discuss the electronic properties of the adsorbed TM on the Cu site of $Cu_2N/Cu(100)$. Our calculations for the pristine surface show that the Cu and N atoms in the Cu_2N layer have charges $q_{Cu} = +0.2$ and $q_N = -0.4$. The adsorption of the TM atom results in a charge transfer mostly from the TM s orbitals to the N ligands, increasing their negative charge. The TM atoms lose practically all the $4s$ electrons. The outermost electrons are thereby in the d shell.

A naive interpretation of the picture that arises from the use of quantized spin models to describe these systems would lead us to conclude that the charge in the d shell of the TM is quantized. Our calculations show that this is not the case. A hint of this can be already seen by inspection of the spin-resolved density of states projected over the d orbitals of the adsorbed TM atoms, shown in Fig. 4, obtained with QE, for the small cell. For instance, the occupancy of the majority spins (left panel) is not 5 for Ni and Co. The presence of very broad peaks indicates strong hybridization of some of the d orbitals with the rest of the system, as we show below.

In Fig. 5 we show the integrated density of states up to the Fermi energy, that gives the occupation of the d shell for the different TM atoms, using both GGA and GGA $+ U$, for several values of U. The results are plotted together with the charge of the isolated atom. In all instances we find that the d shell is more charged than in the free atom case.

The difference between the computed charge and isolated charge, Δq, is shown in the inset for $U = 0$ and $U = 5$ eV. Expectedly, increasing U reduces Δq. Interestingly, Δq increases as we move away from half filling (the Mn atom). Varying U does not yield large changes in these results, except for the Mn atom, in line with results obtained in Ref. [33] for Co and Mn. We have also verified that Δq is stable with respect to changes in the size of the supercell.

FIG. 3. (Color online) Comparative study of structural properties of TM atoms on Cu_2N. (a) Distance form the TM atom to the nearest neighbors N atoms d_N as a function of the TM atom. (b) Distance from the TM atom to the Cu atom lying just below the magnetic atom (d_{Cu}). (c) Distance from the TM atom to the Cu_2N surface (z) as a function of the TM atom. (d) Angle formed by the N-TM-N trimer. The blue (red) line shows the result with the small (big) cell.
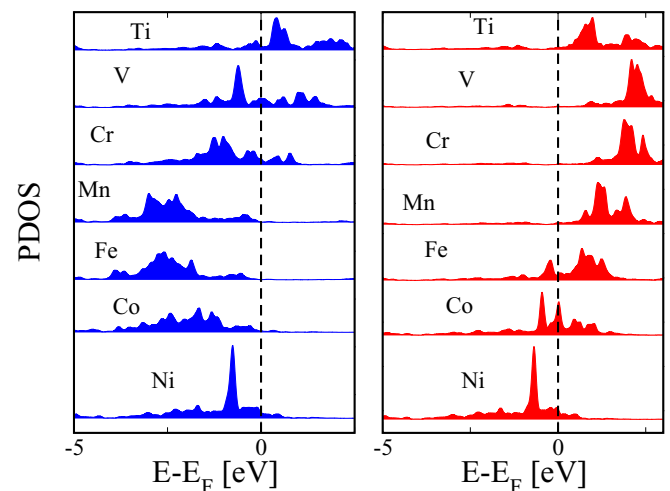

FIG. 4. (Color online) (a) DOS projected (PDOS) over d-orbitals of the different magnetic atoms, for majority spin (left panel) and minority spin (right panel). The results shown correspond to $U = 0$.
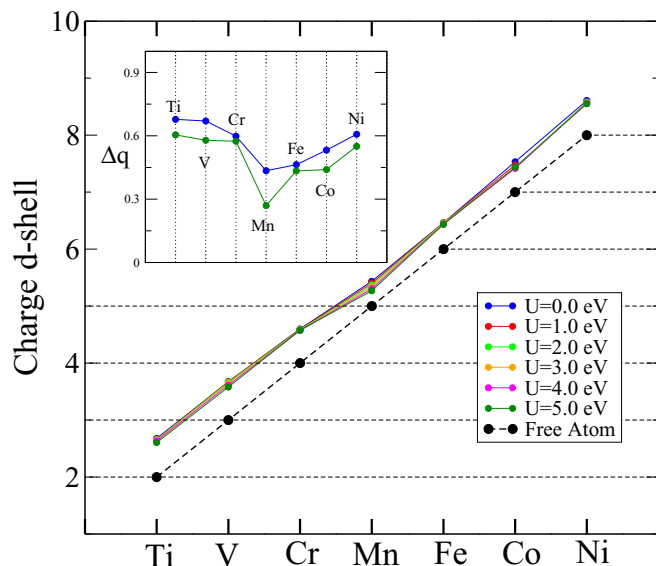
FIG. 5. (Color online) GGA + U calculation of the total charge of the 3d levels for the different TM atoms and different values of U. The black dashed line shows the result for the isolated atoms. Inset: deviation of the charge in the d levels with respect to the isolated atom.

D. Magnetic properties

We now discuss the evolution of the magnetic moments, μ, of the series of 3d TM adsorbed atoms. In Fig. 6, we show the magnetic moment of the free atoms, μ_{free}, as given by Hund's rule. The largest free atom moment is $\mu = 5\mu_B$, for the half-filled shell (Mn) and goes down as we move away from half filling. The upper panel of Fig 6 shows the GGA + U calculation of the magnetic moment of the TM atoms. With the only exception of Cr, the magnetic moment for the adsorbed TM is always smaller than the free atom case. The deviations
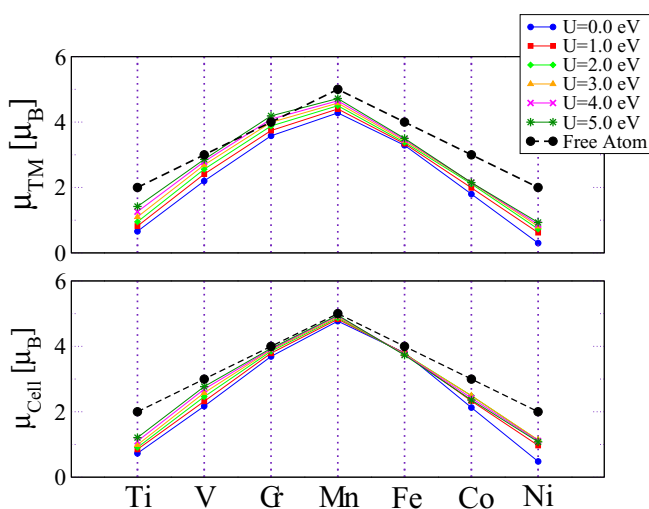

FIG. 6. (Color online) GGA + U calculation of magnetic moment of the TM atoms (in units of μ_B), for different values of of U. (a) Atomic. (b) Unit cell. In both panels the black dashed line shows the expected magnetic moment for the free (isolated) atom (μ_{free}).
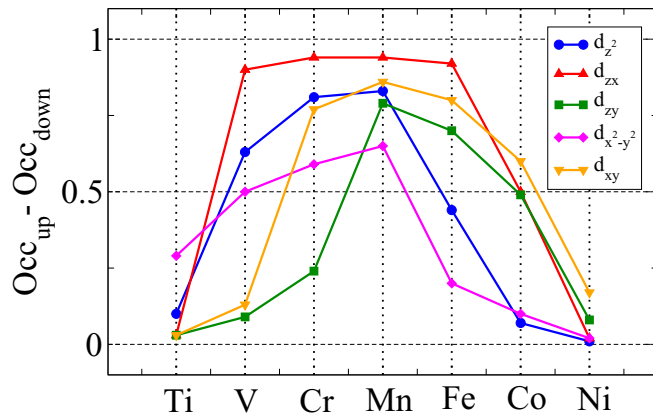

FIG. 7. (Color online) Orbital breakdown of the spin polarization, calculated using the small cell and $U = 0$.

become particularly severe as we move away from half filling. For instance, the magnetic moment of adsorbed Ni is half the value of the free atom case. In contrast with the case of Δq, the value of the magnetic moment depends more strongly on the value of U, yet the atomic limit is only reached in the case of Cr for $U = 5$ eV.

Whereas most of the spin is localized on the magnetic atoms, a substantial amount of the spin density is not located at the d levels of the atom. Therefore, we also plot the cell magnetic moments and compared them with the free atom case [see Fig. 6(b)]. It is apparent that, in the case of the cell moment, the deviations from the free case are very small for V, Cr, Mn, and Fe. In the case of Ti and Ni, the deviation from the free case is still a factor of 2. The overall trend is that, close to half-filling, our DFT results are closer to the free case, where it is assumed that the s shell is completely filled and the d electrons are in the high spin configuration. It is worth noting that this last assumption is not true for a free Cr atom, whose $4s^2$ state is not the ground state but an excited one.

Figure 7 shows the spin polarization of the different d orbitals as a function of the TM atom. Whereas at half filling the magnetic moment has to be evenly distributed in the 5 d orbitals, away from half filling this is no longer the case. The orbital composition of the magnetization is interesting because it affects the magnetic anisotropy and because only one of the d orbitals, the d_z^2, couples to the s orbital of the last atom in the STM tip. This result is particularly interesting in the case of Ti, Co, and Ni where we can appreciate that the d_z^2 orbital

TABLE I. DFT calculation of the spin polarization for $U = 5$ eV.

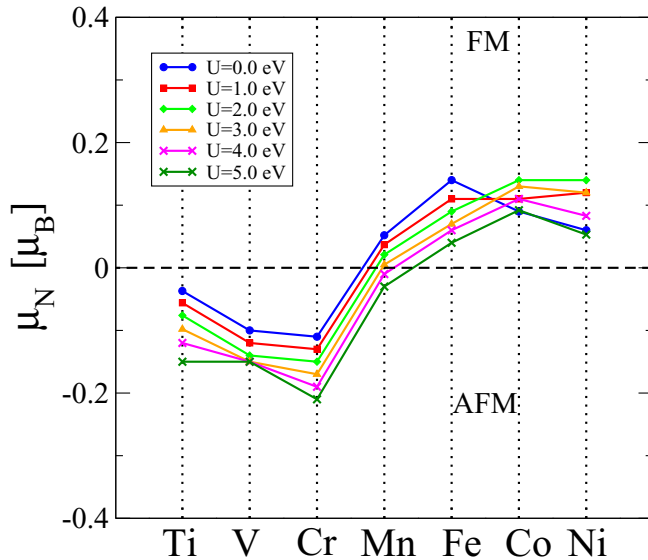| Atom | Spin polarization of TM atoms | | | |
	d shell	TM atom	Cell	Free atom
Ti	0.62	0.71	0.6	1
V	1.32	1.45	1.41	1.5
Cr	1.98	2.10	1.97	2
Mn	2.25	2.36	2.47	2.5
Fe	1.62	1.75	1.91	2
Co	1.05	1.1	1.25	1.5
Ni	0.46	0.47	0.57	1

FIG. 8. (Color online) GGA $+ U$ calculation of the magnetic moment of the nearest-neighbor N atom as a function of the TM atom, for different values of U.

has a very small spin polarization. These calculations were performed for the small cell, so we should expect interesting features in STM experiments when dealing with Co and Ni chains [17].

The difference between the atomic and the cell magnetizations, summarized in Table I, implies that the surrounding atoms gain some magnetic moment as well. Our results, shown in Fig. 8, also show that their alignment with the N atoms can be both ferromagnetic (FM) or antiferromagnetic (AFM) depending on the TM. In particular, the correlation is AFM below half filling and FM above half filling. At half filling the results depend on the value of U. Below we provide an explanation to this sign, based on a zero bandwidth multi-orbital Anderson model.

Finally, calculations for Co atoms were performed using ELK for different values of U in order to check the magnetic properties obtained with QE. The results obtained with both codes were in very good agreement.

III. CONNECTION WITH THE SPIN MODELS

The DFT results of the previous section clearly show that the charge and spin of the d shells are not quantized. There is thus an apparent conflict between the DFT calculations and the use of spin Hamiltonian models with quantized spins [1,2,18]. In this section we address this important topic and provide a solution for this conundrum. First, we build a zero bandwidth multi-orbital Anderson model starting from the DFT results. The zero bandwidth Anderson model describes the d orbitals of the TM atom, their hybridization to their neighbors, the crystal field splitting due to electrostatic interactions, intrashell Coulomb repulsion, and the spin-orbit coupling (SOC). Most of these parameters are obtained from the DFT calculations, as we discuss below. Second, we solve the Anderson model exactly within a restricted multiparticle Hilbert space that includes both $d^n p^{12}$ and $d^{n+1} p^{11}$ configurations, where d^n

stands for n electrons in the d shell of the TM and the p^m stands for m electrons in the p shells of the nitrogen first neighbors (without charge transfer there are six electrons in each p shell of the N atoms). Charge fluctuations were shown to be important in the case of cobalt adatoms on MgO/Ag [61]. Including charge fluctuations in the zero bandwidth Anderson model gives rise to a noninteger occupation of the d shell but still preserves many-body states with a quantized spin S, that is identified with the spin of the quantum spin Hamiltonians.

A. Maximally localized Wannier functions as atomic-like basis set

The derivation of an effective zero bandwidth Anderson model starting from the DFT calculations requires a representation of the Kohn-Sham Hamiltonian in a basis set that contains atomic-like d states localized around the transition metal atom. Our DFT calculations are performed with a plane-wave basis whereas the zero bandwidth multi-orbital Anderson Hamiltonian demands a local basis. Thus, to go from plane wave to a local basis, we represent the DFT Kohn-Sham Hamiltonian in the basis of maximally localized Wannier functions (MLWFs) [54–57,59,62], computed using the code WANNIER90, as described in Ref. [57].

The computation of the MLWFs is implemented as follows. First, we select a group of Bloch bands from a spin unpolarized [63] calculation for a given TM/Cu$_2$N system. An energy window of 16 eV around the Fermi energy is taken, and the band disentanglement procedure is performed. The selected Bloch bands are initially projected over the s, p, and d orbitals of both the TM atom and the copper atoms and over the p and s orbitals of the nitrogen atoms. The total number of states involved in this procedure is 313, corresponding to the 4 nitrogen atoms (4 orbitals each), 32 copper atoms, and the TM atom (9 orbitals each).

An iterative procedure yields a total of 313 MLWFs including three p-like and five d-like MLWFs localized around the nitrogen atoms and the TM atom respectively. They are shown in Figs. 9 and 10, where two different isosurfaces of the MLWFs with y and $x^2 - y^2$, for Fe and Co, are represented. In the case of isosurfaces with larger value, corresponding to the wave function close to atomic cores, these MLWFs have the same symmetry as the real spherical harmonics with $L = 1$ and $L = 2$. In comparison, the isosurfaces with small value do not show the symmetry of the Cartesian atomic orbitals.

The zero bandwidth Anderson model is build in a basis of single-particle states that involves the five d orbitals of the TM and the six p orbitals of the two first-neighbor nitrogen atoms. The representation of the Kohn-Sham Hamiltonian H_{KS} in this basis can be written as

$$H_{\text{CF}} + H_{\text{hyb}} = \begin{pmatrix} H_{dd} & H_{dp} \\ H_{pd} & H_{pp} \end{pmatrix}, \qquad (1)$$

where we identify the crystal field Hamiltonian for the d orbitals $H_{\text{CF}} = H_{dd}$ and the pd hybridization Hamiltonian with the off-diagonal blocks H_{dp} and H_{pd}. Importantly, Figs. 9 and 10 show how the MLWFs for cobalt have bigger overlap with the MLWFs of the N atom than those of Fe, both for the $x^2 - y^2$ and y orbitals. This accounts for the fact that the hybridization between the TM d orbitals and nitrogen p
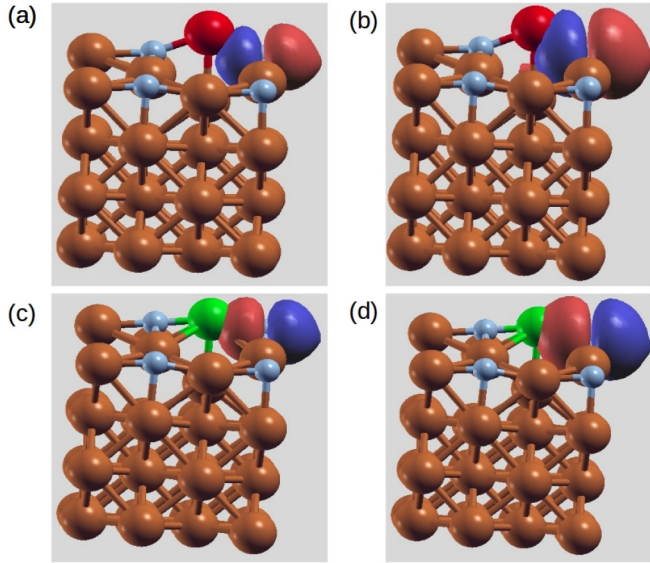
FIG. 9. (Color online) Wannier orbitals for Fe and Co atoms at Cu_2N. (a) p_y orbital of a nearest-neighbor N atom for Fe at Cu_2N close to the atom (isosurface 3). (b) p_y orbital of a nearest-neighbor N atom for Fe at Cu_2N far from the atom (isosurface 1). (c) p_y orbital of a nearest-neighbor N atom for Co at Cu_2N close to the atom (isosurface 3). (d) p_y orbital of a nearest neighbor N atom for Co at Cu_2N far from the atom (isosurface 1).

orbitals is larger for Co than for Fe. In particular, the matrix element $\langle x^2 - y^2|H_{KS}|y\rangle$ is twice as large for Co than for Fe.
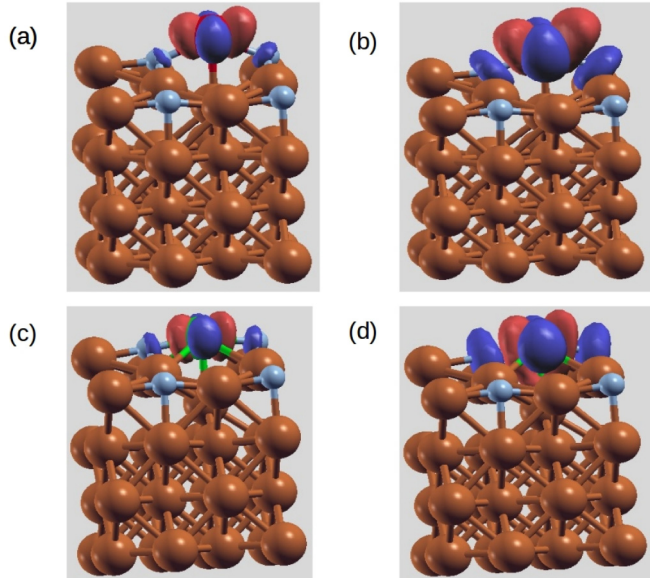

FIG. 10. (Color online) Wannier orbitals for Fe and Co atoms at Cu_2N. (a) $d_{x^2-y^2}$ orbital of a nearest-neighbor N atom for Fe at Cu_2N close to the atom (isosurface 3). (b) $d_{x^2-y^2}$ orbital of a nearest-neighbor N atom for Fe at Cu_2N far from the atom (isosurface 1). (c) $d_{x^2-y^2}$ orbital of a nearest-neighbor N atom for Co at Cu_2N close to the atom (isosurface 3). (d) $d_{x^2-y^2}$ orbital of a nearest-neighbor N atom for Co at Cu_2N far from the atom (isosurface 1).

B. Zero bandwidth multi-orbital Anderson model

We now introduce the zero bandwidth multi-orbital Anderson model for the TM on the Cu_2N substrate describing the electrons in the five d orbitals hybridized with the p orbitals of the two adjacent N atoms. The Hamiltonian is the sum of four terms: the Kohn-Sham Hamiltonian of the previous section, plus the Coulomb repulsion of the electrons in the d shell, the Coulomb attraction of the d levels with the TM nucleus, and their spin-orbit coupling:

$$H = H_{KS} + H_{Coul} + H_Z + H_{SO}. \tag{2}$$

In the following we label the five d-like MLWFs of the TM with the index m, and six p-like MLWFs of the two nitrogen atoms with the index n. The second quantization representation of the first term reads

$$H_{KS} + H_Z = \sum_{m,m',\sigma} (\langle m|H_{KS}|m'\rangle + E_d\delta_{m,m'})d^\dagger_{m\sigma}d_{m'\sigma}$$
$$+ \sum_{n,n',\sigma} \langle n|H_{KS}|n'\rangle p^\dagger_{n\sigma}p_{n'\sigma}$$
$$+ \sum_{m,n,\sigma} (\langle m|H_{KS}|n\rangle d^\dagger_{m\sigma}p_{n\sigma} + \text{H.c.}). \tag{3}$$

The matrix $H_{dd} = \sum_{m,m',\sigma} \langle m|H_{KS}|m'\rangle$ describes the crystal field [63]. The E_d energy scale accounts for the Coulomb interaction with the positive charge in the nucleus and has to be included to offset the excess in the Coulomb repulsion in the configurations d^{n+1} with an extra electron [64]. The matrix $H_{pp} = \langle n|H_{KS}|n'\rangle$ describes the single-particle p levels of the first-neighbor nitrogen atoms and $H_{dp} = \langle m|H_{KS}|n\rangle$ describes their hybridization with the d levels, responsible for the charge fluctuation. H_{dd}, H_{pp}, and H_{pd} are obtained from the DFT Hamiltonian using the Wannierization procedure described above.

The electron-electron Coulomb repulsion in the d shell reads

$$H_{Coul} = \frac{1}{2} \sum_{\substack{m,m'\\m'',m'''}} V_{mm''m'm'''} \sum_{\sigma\sigma'} d^\dagger_{m\sigma}d^\dagger_{m''\sigma'}d_{m'''\sigma'}d_{m'\sigma}. \tag{4}$$

For the evaluation of the Coulomb integrals $V_{mm''m'm'''}$ we transform the angular part to a basis of eigenstates of $\ell = 2$. For the radial part we take an effective radial hydrogen-like function (with effective charge Z and a effective Bohr radius a_μ) to avoid the otherwise cumbersome numerical integration of the actual Wannier functions. In the basis of eigenstates of $\ell = 2$, all the Coulomb integrals scale linearly with the value of $V_{0000} \equiv U$ [63]. Although the numerical evaluation of U in terms of the parameters Z and a_μ is straightforward, for the sake of generality U will be considered a parameter, taken to satisfy the atomic Hund's rule. For a given choice of U, E_d is adjusted so that the average charge in the ground state of the many-body calculation described below equals the charge obtained in the DFT calculations.

The spin-orbit term in the TM reads

$$H_{SO} = \lambda_{SO} \sum_{mm',\sigma\sigma'} \langle m\sigma|\vec{\ell} \cdot \vec{S}|m'\sigma'\rangle d^\dagger_{m\sigma}d_{m'\sigma'}, \tag{5}$$

where λ_{SO} is the atomic spin-orbit coupling of the d electrons. This term is the only one that does not commute with the total spin operator and is the ultimate responsible of the lifting of the $2S + 1$ degeneracy of the spin multiplets.

In the following we shall show results for the case of Fe on Cu$_2$N. Given the small size of the single-particle basis (five d orbitals and six p orbitals) and the fact that we restrict the Hilbert space to the configurations $d^n p^{12}$ and $d^{n+1} p^{11}$, with $n = 6$ for Fe, with a total of 1650 multi-electron states, the zero bandwidth multi-orbital Anderson model can be solved by exact numerical diagonalization.

C. Effective spin model

In the seminal work [2] of Hirjibehedin *et al.*, the spin excitations measured with STM-IETS were found to be described with the following spin Hamiltonian:

$$H = D(\vec{e}_1 \cdot \vec{S})^2 + E[(\vec{e}_2 \cdot \vec{S})^2 - (\vec{e}_3 \cdot \vec{S})^2] \quad (6)$$

with $S = 2$ and $\vec{e}_1 = (0,1,0)$ along the nitrogen direction, and $\vec{e}_2$ and $\vec{e}_3$ are the off-plane and the hollow directions. The experimental results could be fitted with $D = -1.55$ meV and $E = 0.31$ meV. Thus, the wave function of the ground state and first excited state would be given by linear combinations of the rates of $|2, \pm 2\rangle$, with a small mixing with the state $|2,0\rangle$ in the case of the ground state. The height of the inelastic steps was found to be related to the matrix elements of the spin operators, giving additional support to the notion that the quantized spin Hamiltonian (6) provides a quite good description of the spin excitations of iron on this surface. Recent experiments [14] with a detailed study of the IETS of single Fe/Cu$_2$N as a function of the three components of the magnetic field show that the addition of extra terms in the Hamiltonian (6) yields an even better agreement with the experiment. Spin chains formed with Fe atoms in this system can also be modeled successfully with this Hamiltonian and the addition of interatomic Heisenberg coupling [8,11]. Altogether, these results support the notion that Fe can be described with a quantized anisotropic spin $S = 2$.

D. Adiabatic continuity and spin conservation argument

We now address the crucial question: Given that according to DFT both charge and spin of the d electrons in the transition metal are *not* quantized, what is the origin of the quantized spin in the model Hamiltonian? We now show that the quantized spin belongs to the many-body wave function that combines configurations with different charge states in the d shell. In the case of Fe, these would be configurations $d^6 p^{12}$ with $S^{(d)} = 2$ and configurations with $d^7 p^{11}$ and $S^{(d)} = \frac{3}{2}$, where $S^{(d)}$ is the spin of the d electrons. These many-body states yield noninteger charge and magnetic moment in the TM, in agreement with DFT, but they have a well defined *total* quantized spin, in agreement with the spin quantized models. This is strictly true in the absence of spin-orbit interactions, and remains true when spin-orbit splittings are much smaller than the energy gap between different multiplets, which we show to be the case in a wide range of parameters.

In order to understand the results of our numerical calculations, it is convenient to recall that atomic iron, with

six d electrons, has a ground state with $S = 2$ and $L = 2$, and a total degeneracy of $(2L + 1)(2S + 1) = 25$. The former ground state is captured by the zero bandwidth multi-orbital Anderson model when switch off the H_{dd} crystal field, the H_{pd} hybridization, the SOC, considering configurations with six electrons. The crystal field H_{dd} quenches the orbital moment, so that in the absence of spin-orbit coupling the ground state of the model has $S = 2$ and no orbital degeneracy. This multiplet is separated from the next higher energy multiplets, also with $S = 2$, by a gap of at least 300 meV, although this number depends on U.

We now discuss the effect of mixing configurations with a different number of electrons in the d shell. On one hand, the relative weight of the configurations $d^6 p^{12}$ and $d^7 p^{11}$ depends on U, which is taken to be $U = 5.5$ eV in line with recent calculations for Co/Cu(100) [65]. On the other hand, H_{pp}, H_{dd}, H_{pd} are obtained from DFT and E_d remains as the only
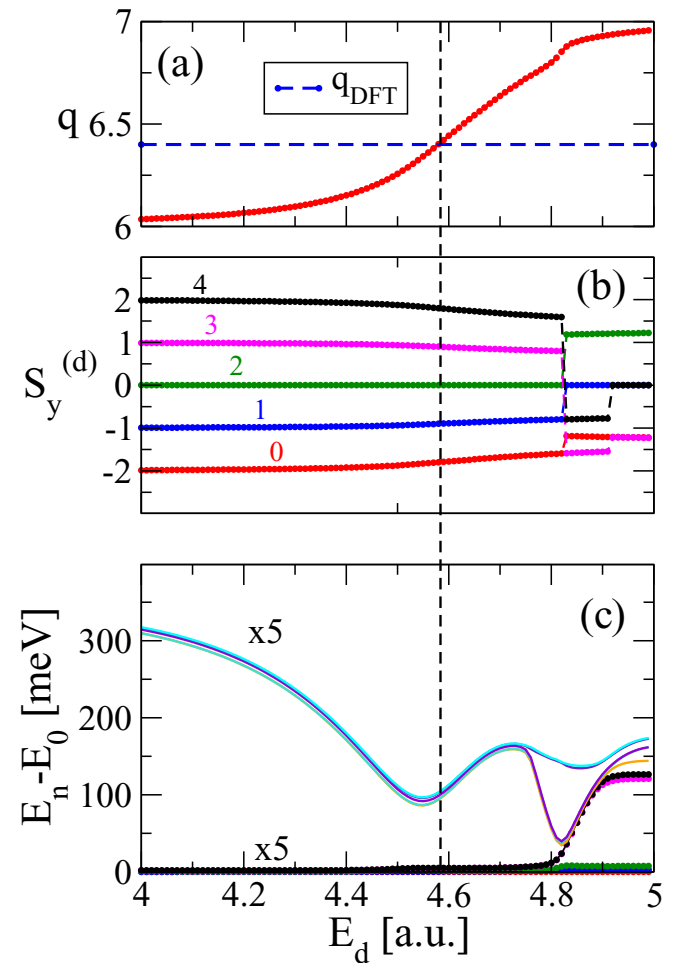

FIG. 11. (Color online) Numerical diagonalization of the zero bandwidth multi-orbital Anderson model for the Fe atom at Cu$_2$N. (a) Average charge of the d levels of the Fe atom for the ground state as a function of E_d in atomic units ($U = 5.5$ eV and $\lambda_{SO} = 50$ meV). (b) S_y (y is the N atom's axis) of the d electrons for the five lowest eigenvalues as a function of E_d ($U = 5.5$ eV and $\lambda_{SO} = 0$). (c) Excitation energies corresponding, for small E_d, to the two lowest multiplets with $S = 2$, as a function of E_d ($U = 5.5$ eV and $\lambda_{SO} = 50$ meV).

adjustable parameter in the calculation. We start with a value of E_d so that the charge at Fe is $q = 6$ and ramp up E_d, so that q increases, as shown in Fig. 11(a). In Fig. 11(c) we plot the evolution of the excitation energies as a function of E_d. For $q = 6$ the ground state has a multiplicity of 5. The next multiplet lies 300 meV above. As we ramp up q, these two multiplets remain well separated in energy, quite beyond the point where $q = 6.4$, the value obtained from DFT. We thus see that the ground state multiplet at $q = 6.4$ is *adiabatically connected* to the ground state multiplet at $q = 6$. The effect of spin-orbit coupling, that we discuss in detail below, is to create a small splitting and to mix different states within the multiplet as E_d is varied, implying a change in the magnetic anisotropy tensor.

The total spin is preserved as we ramp E_d. However, by changing the relative weight of $d^6 p^{12}$ and $d^7 p^{11}$ configurations, the magnetic moment in the d levels is expected to be reduced, moving from $S(d) = 2$ towards $S(d) = 3/2$. This is reflected in our calculations [see Fig. 11(b)], taking $\lambda_{SO} = 0$ and a finite magnetic field B_y that lifts the $2S + 1$ degeneracy. As E_d is increased, the expectation value of the operator describing the spin of the d electrons along the y axis, $S_y^{(d)}$, calculated with the five lowest energy states, evolves from the eigenstates of S_y for $S = 2$ to nonquantized values, in agreement with DFT results.

Further increase of E_d yields that the mixing between $d^6 p^{12}$ and $d^7 p^{11}$ is so large that the splitting between the ground state $S = 2$ multiplet and the first excited multiplet vanishes. When such regime is reached, the spin of the ground state changes, breaking the adiabatic connection with the state with $S = 2$ and quantized charge. In our calculations this happens for $q \simeq 6.8$, larger than the DFT charge, $q > 6.4$. Thus, the model captures the crossover from the weak coupling limit, where the ground state is adiabatically connected with the $q = 6, S = 2$, state, to the strong coupling limit in which the spin of the ground state multiplet changes and the adiabatic connection is lost.

E. TM-nitrogen spin correlation

The fact that the quantized spin corresponds to configurations with two charge states involving both d electrons in the TM and p electrons in the first-neighbor nitrogen atoms has implications on the spin correlation of the TM and N magnetic moments. Since both $d^n p^{12}$ and $d^{n+1} p^{11}$ have the same total spin, we have $S(d^n) = S_T = S(d^{n+1}) \pm \frac{1}{2}$. The sign, and thereby the spin-correlation between the unpaired electron in the ligand and the magnetic moment of the atom, depends on whether $S(d^n)$ is larger or smaller than $S(d^{n+1})$. Thus, for Fe we have that $S(d^6) = 2$ and $S(d^7) = 3/2$, so that the unpaired fermion must couple ferromagnetically with the $S = 3/2$ of the d^7 configuration, to keep $S = 2$. In contrast, for Cr we have $S(d^4) = 2$ mixing with $S(d^5) = 5/2$ configurations to bring up the charge, so that the unpaired fermion in the nitrogen must couple antiferromagnetically with the atomic magnetic moment.

This argument accounts for the trend obtained in our DFT calculations, shown in Fig. 8, where the small magnetization of the first-neighbor nitrogen atoms is antiparallel to the TM magnetic moment for Ti, V, and Cr, and is ferromagnetic in the case of Fe, Co, and Ni. In the case of Mn we obtain both signs,

depending on U. From the argument of the previous paragraph we would expect a ferromagnetic coupling. Incidentally, the same argument can be applied to the conventional Anderson model with $S = 1/2$, predicting correctly the well known [44] antiferromagnetic interaction between the local moment and the adjacent electrons.

F. Spin-orbit coupling, magnetic anisotropy, and symmetry of the wave functions

The discussion above has ignored the role of spin-orbit coupling, even if the numerical results shown in Figs. 11(a) and 11(c) are obtained with a spin orbit coupling $\lambda_{SO} = 50$ meV. These calculations show that the spin-orbit coupling splits the otherwise $(2S + 1)$ degenerate multiplets. However, the splittings between the different multiplets are still much larger than the energy gaps between them, so that a well defined total spin S can be attributed, even in the presence of spin-orbit coupling. The fine structure within the lowest energy multiplet can be described with an effective spin Hamiltonian, like the one in Eq. (6).

We now discuss the symmetry of the wave functions obtained from the exact diagonalization for two values of E_d, corresponding to having either exactly $q = 6$ electrons at the d shell or $q = 6.4$, the average charge obtained from DFT. For that matter, we use the fact that the eigenstates ψ_n of the multi-orbital Hamiltonian can be written as linear combinations of configuration states with well defined
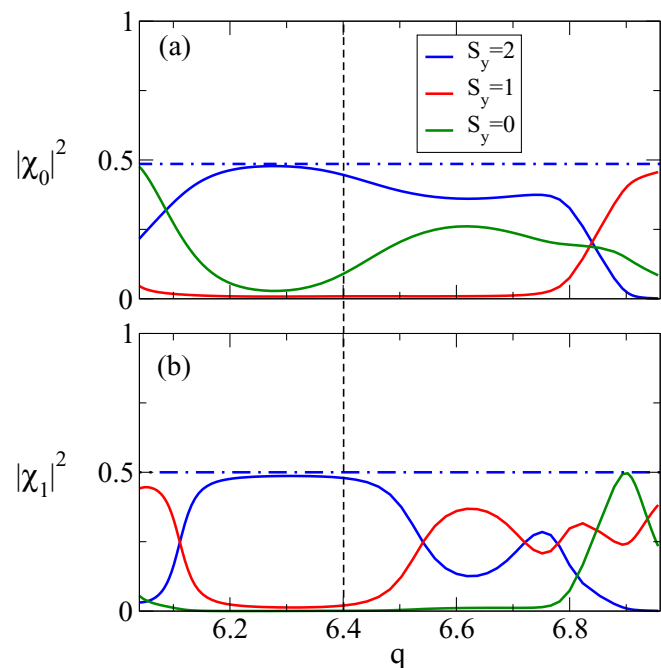

FIG. 12. (Color online) Numerical diagonalization of the zero bandwidth multi-orbital Anderson model for Fe atom at Cu_2N ($U = 5.5$ eV and $\lambda_{SO} = 50$ meV). Eigenvectors projection over S_y for the ground state (upper panel) and the first excited state (lower panel) as a function of the charge in the d shell. Blue lines show projection over $|\pm2\rangle$, red lines show projection over $|\pm1\rangle$, and green lines show projection over $|0\rangle$. Blue dashed lines show the projection over $|\pm2\rangle$ obtained from the spin model [2].
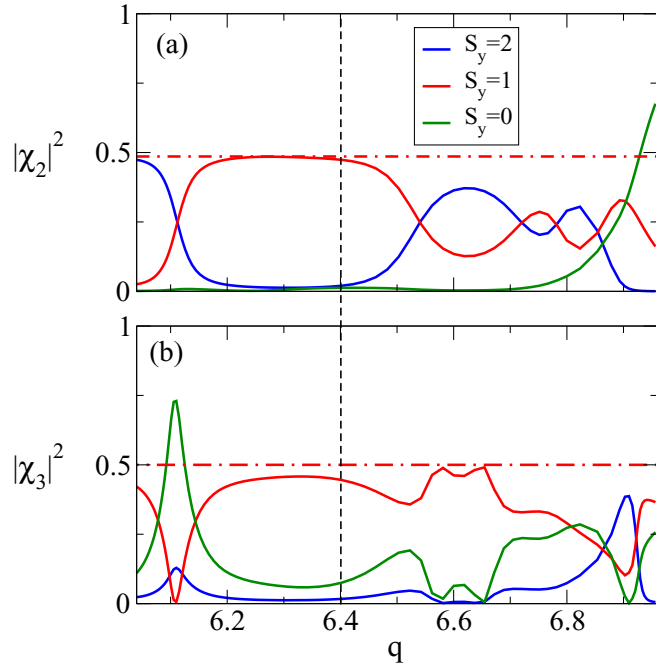
FIG. 13. (Color online) Numerical diagonalization of the zero bandwidth multi-orbital Anderson model for Fe atom at Cu_2N ($U = 5.5$ eV and $\lambda_{SO} = 50$ meV). Eigenvector projections over S_y for the second excited state (upper panel) and the third excited state (lower panel) as a function of the charge in the d shell. Blue lines show projection over $|\pm2\rangle$, red lines show projection over $|\pm1\rangle$, and green lines show projection over $|0\rangle$. Red dashed lines show the projection over $|\pm1\rangle$ obtained from the spin model [2].

total S_y:

$$|\psi_n\rangle = \sum_{S_y,\gamma} \chi_n(\gamma, S_y)|\gamma, S_y\rangle, \tag{7}$$

where γ labels all the other quantum number necessary to characterize the basis set. In Figs. 12(a), 12(b), 13(a), 13(b), and 14(a) we plot the projection of the five lowest energy states of the zero bandwidth multi-orbital Anderson model over the eigenstates of $|S = 2, S_y\rangle$. In the case of $q = 6$ it is apparent that the ground state wave function is dominated by $S_y = 0$ states, in disagreement with the experiment [see Fig. 12(a)]. The arrangement of the energy levels seems to indicate that the nitrogen direction (y axis) is a hard axis in the problem [$\vec{e}_1 = (0,1,0)$ and $D > 0$ in Eq. (6)]. Given that the charge fluctuations are negligible in this limit, the main contribution to the magnetic anisotropy comes from the interplay between the crystal field term in the Hamiltonian, H_{dd}, and the spin-orbit coupling. Interestingly, when E_d is ramped so that q increases, the content of the wave functions evolves and for $q = 6.4$ the wave functions [Figs. 12, 13, and 14(a)] are in good agreement with those obtained from the spin model [2] in which the nitrogen direction is the easy axis in the problem [$\vec{e}_1 = (0,1,0)$ and $D < 0$ in Eq. (6)]. In particular, we note that the five lowest energy states of the Anderson model have wave functions with strong overlap with those of the effective spin Hamiltonian [2]. We thus see that the ligand field contribution, coming from the dp hybridization, changes qualitatively the magnetic anisotropy tensor. Interestingly, in
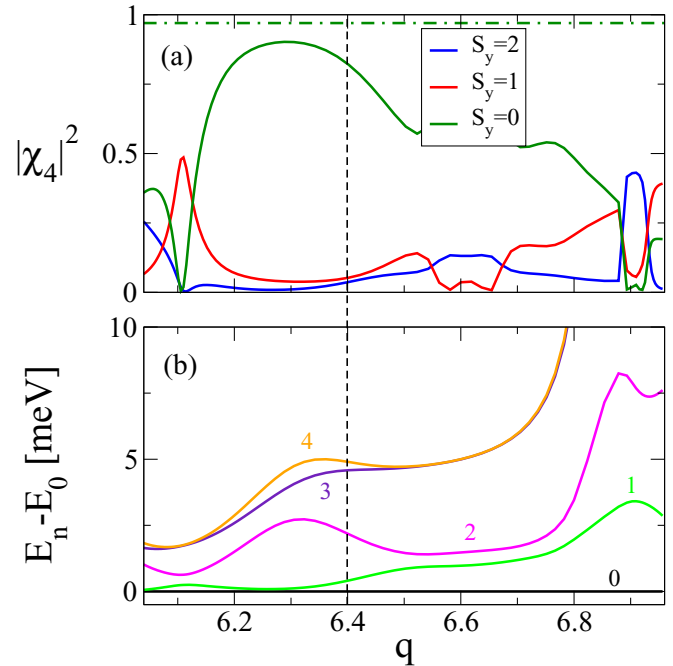

FIG. 14. (Color online) Numerical diagonalization of the zero bandwidth multi-orbital Anderson model for the Fe atom at Cu_2N ($U = 5.5$ eV and $\lambda_{SO} = 50$ meV). (a) Eigenvector projections over S_y for the fourth excited state as a function of the charge in the d shell. Blue lines show projection over $|\pm2\rangle$, red lines show projection over $|\pm1\rangle$, and green lines show projection over $|0\rangle$. Green dashed lines show the projection over $|0\rangle$ obtained from the spin model [2]. (b) Low energy spectrum as a function of the charge in the d shell.

the case of Fe/Cu_2N we find that the inclusion of charge fluctuations is essential to capture the correct easy axis within the zero bandwidth multi-orbital Anderson model.

We finally analyze the low energy excitation spectrum, $E_n - E_0$, where E_0 is the energy of the ground state. In the range of E_d considered, such that q moves from the nominal value $q = 6$ to the DFT value $q = 6.4$, the five energy levels of the lowest energy multiplet are always split. This is expected in the case of a integer spin ($S = 2$) described with Hamiltonian Eq. (6). Interestingly, the low energy splittings increase as q is increased towards the DFT value, as shown in Fig. 14(b). This is related to the fact that the energy gap between the first and second fivefold degenerate multiplets decreases, as shown in Fig. 11(c). This behavior can be understood in terms of degenerate perturbation theory, where spin-orbit coupling only splits the states in the lowest energy multiplet through virtual transitions to the higher state multiplets. We note that the spin excitation energies obtained from our calculation are 25% smaller than those observed in the experiment. So, whereas the model captures the right symmetry, it can only give a rough description of the excitation energies, which is probably due to the approximations in the model, such as the restrictions taken in the many-body Hilbert space.

IV. CONCLUSIONS

In this work we have undertaken a systematic study of the electronic properties of the $3d$ transition metals on the Cu_2N

surface. We systematically find that the charge and spin of the d electrons are not quantized, and are thereby different from the ones in isolated atoms, which is expected given the conducting nature of the substrate. We have then addressed the issue of how to reconcile these results with the fact that quantized spin models account for the spin excitations of Mn, Fe, and Co ad-atoms. For that matter we propose a zero bandwidth multi-orbital Anderson model in which many-body states that mixes configurations with two charge states in the d shell are considered. Importantly, even if the charge is not well defined in the d shell, these multi-electron wave functions have a well defined total spin S. We find that the states with a quantized charge in the d shell are adiabatically connected with the actual many-body states that mix configurations $d^n p^{12}$ and $d^{n+1} p^{11}$ in the sense that both have the same total spin S and there is no mixing with higher energy multiplets as the additional energy is varied numerically.

We thus conclude that quantized spin S of the model actually refers to the spin of these many-body states that include both the d electrons and the ligand electrons. It is thus fair to say that the magnetism in this system is not strictly atomic, which connects with previous results in the case of magnetic atoms on metallic surfaces [66], for which sophisticated theoretical treatments have been proposed [67,68]. Our picture provides a natural explanation of the sign of the spin correlation between the TM and the nitrogen atoms obtained in the DFT calculations and reconciles the use of quantized spin Hamiltonians with the results of DFT calculations. Our Anderson model calculations for Fe/Cu$_2$N also indicate that charge fluctuations in the Fe d shell, due to the hybridization to the ligands, are essential to capture both the symmetry and the magnitude of the magnetic anisotropy observed in the experiment.

Finally, we expect that our analysis should also be applicable to other systems with magnetic adatoms and molecules deposited in conducting surfaces whose spin excitations can be described in terms of quantized spin models [66,69–72].

[1] C. F. Hirjibehedin, C. P. Lutz, and A. J. Heinrich, Science **312**, 1021 (2006).

[2] C. Hirjibehedin, C-Y Lin, A. F. Otte, M. Ternes, C. P. Lutz, B. A. Jones, and A. J. Heinrich, Science **317**, 1199 (2007).

[3] A. F. Otte, M. Ternes, K. von BErgmann, S. Loth, H. Brune, C. P. Lutz, C. F. Hirjibehedin, and A. J. Heinrich, Nat. Phys. **4**, 847 (2008).

[4] A. F. Otte, M. Ternes, S. Loth, C. P. Lutz, C. F. Hirjibehedin, and A. J. Heinrich, Phys. Rev. Lett. **103**, 107203 (2009).

[5] S. Loth, K. von Bergmann, M. Ternes, A. F. Otte, C. P. Lutz, and A. J. Heinrich, Nat. Phys. **6**, 340 (2010).

[6] S. Loth, M. Etzkorn, C. P. Lutz, D. M. Eigler, and A. J. Heinrich, Science **329**, 1628 (2010).

[7] S. Loth, S. Baumann, C. Lutz, D. Eigler, and A. J. Heinrich, Science **335**, 196 (2012).

[8] B. Bryant, A. Spinelli, J. J. T. Wagenaar, M. Gerrits, and A. F. Otte, Phys. Rev. Lett. **111**, 127203 (2013).

[9] J. C. Oberg, M. Reyes Calvo, F. Delgado, M. Moro-Lagares, D. Serrate, D. Jacob, J. Fernández-Rossier, and C. F. Hirjibehedin, Nat. Nanotechnol. **9**, 64 (2013).

[10] T. Choi and J. A. Gupta, J. Phys.: Condens. Matter **26**, 394009 (2014).

[11] A. Spinelli, B. Bryant, F. Delgado, J. Fernández-Rossier, and A. F. Otte, Nat. Mater. **13**, 782 (2014).

[12] A. Spinelli, M. Gerrits, R. Toskovic, B. Bryant, M. Ternes, and A. F. Otte, arXiv:1411.4415.

[13] S. Yan, D-J. Choi, J. A. J. Burgess, S. Rolf-Pissarczyk, and S. Loth, Nat. Nanotechnol. **10**, 40 (2015).

[14] S. Yan, D.-J. Choi, J. A. J. Burgess, S. Rolf-Pissarczyk, and S. Loth, Nano Lett. **15**, 1938 (2015).

[15] A. Heinrich, Phys. Today **68**, 42 (2015).

[16] K. von Bergmann, M. Ternes, S. Loth, C. P. Lutz, and A. J. Heinrich, Phys. Rev. Lett. **114**, 076601 (2015).

[17] B. Bryant, R. Toskovic, A. Ferrón, J. L. Lado, A. Spinelli, J. Fernández-Rossier, and A. F. Otte, Nano Lett. **15**, 6542 (2015).

[18] J. Fernández-Rossier, Phys. Rev. Lett. **102**, 256802 (2009).

[19] J. Fransson, Nano Lett. **9**, 2414 (2009).

[20] J.-P. Gauyacq and N. Lorente, J. Phys.: Condens. Matter **26**, 394005 (2014).

[21] R. Žitko and T. Pruschke, New J. Phys. **12**, 063040 (2010).

[22] F. Delgado, J. J. Palacios, and J. Fernández-Rossier, Phys. Rev. Lett. **104**, 026601 (2010).

[23] F. Delgado and J. Fernández-Rossier, Phys. Rev. B **82**, 134414 (2010).

[24] F. Delgado, C. F. Hirjibehedin, and J. Fernández-Rossier, Surf. Sci. **630**, 337 (2014).

[25] A. Hurley, N. Baadji, and S. Sanvito, Phys. Rev. B **84**, 115435 (2011).

[26] M. Ternes, New J. Phys. **17**, 063016 (2015).

[27] F. Delgado and J. Fernández-Rossier, Phys. Rev. B **84**, 045439 (2011).

[28] A. B. Shick, F. Máca, and A. I. Lichtenstein, Phys. Rev. B **79**, 172409 (2009).

[29] A. N. Rudenko, V. V. Mazurenko, V. I. Anisimov, and A. I. Lichtenstein, Phys. Rev. B **79**, 144418 (2009).

[30] N. Lorente and J. P. Gauyacq, Phys. Rev. Lett. **103**, 176601 (2009).

[31] J. W. Nicklas, A. Wadelhra, and J. W. Wilkins, J. Appl. Phys. **110**, 123915 (2011).

[32] M. C. Urdaniz, M. A. Barral, and A. M. Llois, Phys. Rev. B **86**, 245416 (2012).

[33] C-Y. Lin and B. A. Jones, Phys. Rev. B **83**, 014413 (2011).

[34] R. Pushpa, J. Cruz, and B. A. Jones, Phys. Rev. B **84**, 075422 (2011).

[35] M. C. Urdaniz, M. A. Barral, A. M. Llois, and A. Saúl, Phys. Rev. B **90**, 195423 (2014).

[36] M. Persson, Phys. Rev. Lett. **103**, 050801 (2009).

[37] B. Sothmann and J. Koenig, New J. Phys. **12**, 083028 (2010).

[38] J. Fransson, O. Eriksson, and A. V. Balatsky, Phys. Rev. B **81**, 115454 (2010).

[39] J. P. Gauyacq, N. Lorente, and F. D. Novaes, Prog. Surf. Sci. **87**, 63 (2012).

[40] F. Delgado, S. Loth, M. Zielinskg, J. Fernández-Rossier, Europhys. Lett. **109**, 57001 (2015).

[41] E. C. Goldberg and F. Flores, Phys. Rev. B **91**, 165408 (2015).

[42] R. Žitko, R. Peters, and T. Pruschke, New J. Phys. **11**, 053003 (2009).

[43] R. Žitko, Phys. Rev. B **84**, 195116 (2011).

[44] J. R. Schrieffer and P. A. Wolff, Phys. Rev. **149**, 491 (1966).

[45] P. W. Anderson, Phys. Rev. Lett. **17**, 95 (1966).

[46] J. A. Appelbaum, Phys. Rev. **154**, 633 (1967).

[47] P. W. Anderson, Phys. Rev. **124**, 41 (1961).

[48] J. P. Perdew, K. Burke, and M. Ernzerhof, Phys. Rev. Lett. **77**, 3865 (1996).

[49] P. E. Blochl, Phys. Rev. B **50**, 17953 (1994).

[50] P. Giannozzi *et al.*, J. Phys.: Condens. Matter **21**, 395502 (2009).

[51] J. P. Perdew and A. Zunger, Phys. Rev. B **23**, 5048 (1981).

[52] http://elk.sourceforge.net/.

[53] F. Bultmark, F. Cricchio, O. Grånäs, and L. Nordström, Phys. Rev. B **80**, 035121 (2009).

[54] N. Marzari and D. Vanderbilt, Phys. Rev. B **56**, 12847 (1997).

[55] I. Souza, N. Marzari, and D. Vanderbilt, Phys. Rev. B **65**, 035109 (2001).

[56] N. Marzari, A. A. Mostofi, J. R. Yates, I. Souza, and D. Vanderbilt, Rev. Mod. Phys. **84**, 1419 (2012).

[57] A. A. Mostofi, J. R. Yates, Y.-S. Lee, I. Souza, D. Vanderbilt, and N. Marzari, Comput. Phys. Commun. **178**, 685 (2008).

[58] M. Shelley, N. Poilvert, A. A. Mostofi, and N. Marzari, Comput. Phys. Commun. **182**, 2174 (2011).

[59] R. Korytár, M. Pruneda, J. Junquera, P. Ordejón, and N. Lorente, J. Phys.: Condens. Matter **22**, 385601 (2010).

[60] F. D. Novaes, N. Lorente, and J-P. Gauyacq, Phys. Rev. B **82**, 155401 (2010).

[61] I. G. Rau, S. Baumann, S. Rusponi, F. Donati, S. Stepanow, L. Gragnaniello, J. Dreiser, C. Piamonteze, F. Nolting, S. Gangopadhyay, O. R. Albertini, R. M. Macfarlane, C. P. Lutz, B. A. Jones, P. Gambardella, A. J. Heinrich, and H. Brune, Science **344**, 988 (2014).

[62] R. Korytár and N. Lorente, J. Phys.: Condens. Matter **23**, 355009 (2011).

[63] A. Ferrón, F. Delgado, and J. Fernández-Rossier, New J. Phys. **17**, 033020 (2015).

[64] B. Surer, M. Troyer, P. Werner, T. O. Wehling, A. M. Läuchli, A. Wilhelm, and A. I. Lichtenstein, Phys. Rev. B **85**, 085114 (2012).

[65] D. Jacob, J. Phys.: Condens. Matter **27**, 245606 (2015).

[66] A. A. Khajetoorians, S. Lounis, B. Chilian, A. T. Costa, L. Zhou, D. L. Mills, J. Wiebe, and R. Wiesendanger, Phys. Rev. Lett. **106**, 037205 (2011).

[67] B. Schweflinghaus, M. dos Santos Dias, A. T. Costa, and S. Lounis, Phys. Rev. B **89**, 235439 (2014).

[68] M. dos Santos Dias, B. Schweflinghaus, S. Blügel, and S. Lounis, Phys. Rev. B **91**, 075405 (2015).

[69] N. Tsukahara, K. I. Noto, M. Ohara, S. Shiraki, N. Takagi, Y. Takata, J. Miyawaki, M. Taguchi, A. Chainani, S. Shin, and M. Kawai, Phys. Rev. Lett. **102**, 167203 (2009).

[70] A. A. Khajetoorians, B. Chilian, J. Wiebe, S. Schuwalow, F. Lechermann, and R. Wiesendanger, Nature (London) **467**, 1084 (2010).

[71] A. A. Khajetoorians, T. Schlenk, B. Schweflinghaus, M. dos Santos Dias, M. Steinbrecher, M. Bouhassoune, S. Lounis, J. Wiebe, and R. Wiesendanger, Phys. Rev. Lett. **111**, 157204 (2013).

[72] P. Jacobson, T. Herden, M. Muenks, G. Laskin, O. Brovko, V. Stepanyuk, M. Ternes, and K. Kern, Nat. Comm. **6**, 8536 (2015).